universe

MDPI

Review

Be/X-Ray Binaries: Phenomenology, Variability, and Accretion Dynamics

Pablo Reig [1,2]

[1] Institute of Astrophysics, Foundation for Research and Technology-Hellas, 71110 Heraklion, Greece; pau@physics.uoc.gr
[2] Physics Department, University of Crete, 71003 Heraklion, Greece

Abstract

Be/X-ray binaries constitute the largest and most diverse subgroup of neutron star high-mass X-ray binaries. These systems feature a rapidly rotating Be star surrounded by a circumstellar decretion disk that serves as the primary reservoir of accreted matter onto a strongly magnetized neutron star. While a few Be/X-ray binaries remain persistently active, the majority manifest as hard X-ray transient sources, becoming detectable only during X-ray outbursts. This review synthesizes current understanding of their rich phenomenology across optical and X-ray wavelengths, focusing on variability ocurring over timescales that span from seconds to years.

Keywords: X-rays binaries; neutron stars; emission line; Be stars

arXiv:2607.18980v1 [astro-ph.HE] 21 Jul 2026

Check for updates

Academic Editor:

Received:
Revised:
Accepted:
Published:

Copyright: © 2026 by the author. Licensee MDPI, Basel, Switzerland. This article is an open access article distributed under the terms and conditions of the Creative Commons Attribution (CC BY) license.

1. Classification of X-Ray Binaries

X-ray binaries consist of a compact object orbiting around a "normal" star. They are "close" binary systems because there exists a transfer of mass from the optical component to the compact object. By "normal" star, it is meant that nuclear burning is still occurring in its interior. The compact object can be a black hole, a neutron star, or a white dwarf, and we refer to them as black-hole binaries (BHBs), neutron star binaries (NSBs), or cataclysmic variables (CVs), respectively. The spectral type of the optical star defines the system as either a low-mass X-ray binary (LMXB) or a high-mass X-ray binary (HMXB). In LMXBs, the spectral type of the optical companion is typically later than *A*, while in HMXBs it is an early-type *B* or late-type *O* star. In HMXBs, the mass of the companion is typically larger than $\sim$8 $M_\odot$. Our Galaxy hosts a few BHBs (only one confirmed: Cyg X–1, plus candidates like Cyg X–3 and SS 433) and about half of the NSBs are found in HMXBs. LMXBs, with the mass of the companion below $\sim$2 $M_\odot$ include the majority of BHBs and half of the NSBs. CVs contain low-mass companions and are normally considered a different class (the term "X-ray binaries" is normally reserved for binaries with neutron stars or black holes).

Neutron star high-mass X-ray binaries (NS-HMXBs) are accretion-powered systems where a neutron star accretes matter from a massive, early-type companion. They rank among the brightest and most variable X-ray sources in the Milky Way and nearby galaxies and serve as key laboratories for high-energy astrophysics by combining several extreme and interacting physical processes in a single observable system. Studies of NS-HMXBs cover a broad range of topics, from accretion physics to stellar evolution and galactic structure, making them central to both high-energy and stellar astrophysics. The vast majority of NS-HMXBs are X-ray binary transient systems.

NS-HMXBs are classified according to the luminosity class of the donor star into supergiant X-ray binaries (SGXBs) and Be/X-ray binaries (BeXBs). In supergiant systems, the neutron star orbits an evolved O or B supergiant whose powerful stellar wind provides the material for accretion, typically through wind capture (low-luminosity SGXBs), although in a few cases, Roche-lobe overflow leads to the formation of an accretion disk and enhanced X-ray emission (high-luminosity SGXBs). This class also includes the fast and highly variable systems known as supergiant fast X-ray transients. This article focuses on the observational properties of Be/X-ray binaries (BeXBs), the most numerous subgroup of NS-HMXBs. In BeXBs, the optical companion is a Be star, characterized by emission lines (most notably the Hα line), an infrared excess (increased flux at longer wavelengths), and a small degree of linear polarization (typically less than 2%). These features arise from a circumstellar disk, also known as decretion disk, around its equatorial plane. The disk forms from material ejected from the stellar photosphere and evolves over years, undergoing formation, growth, and dissipation. When the disk dissipates, emission lines revert to absorption, the infrared excess disappears, and polarization is no longer detected. Since the disk acts as the reservoir of matter for accretion, it fundamentally drives the observed X-ray variability. In other words, the accretion process is governed by the interaction between the neutron star and this decretion disk.

Figure 1 shows a tree diagram that illustrates the different types of X-ray binaries and the mass transfer mechanism. Table 1 lists the Galactic BeXBs with confirmed optical counterparts. Only systems for which at least one optical spectrum is available are included. The EW(Hα) is the maximum value reported in the literature and is normally related to bright X-ray emision. However, note that for some systems, e.g, MAXI J0903–531, RX J1037.5–5647 only one or very few measurements are available and correspond to relatively quiescence X-ray states.

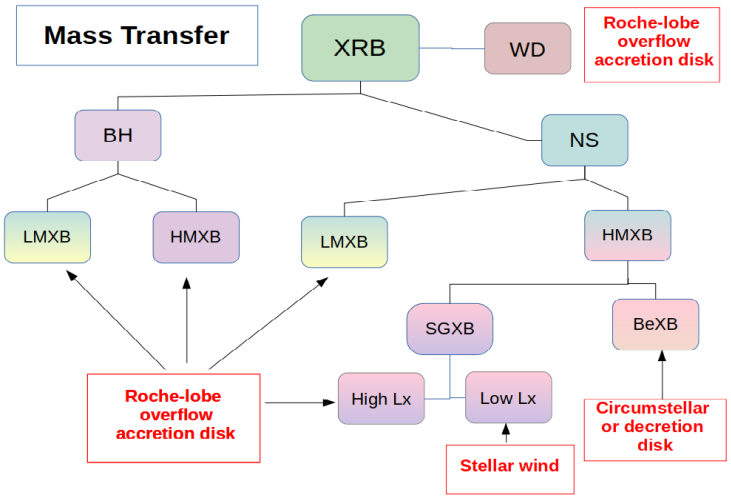

Figure 1. Taxonomy of X-ray binaries

2. A Historical View

Over the past six decades, HMXBs have become central to astrophysics, serving as laboratories for accretion physics, stellar winds, magnetic fields, binary evolution, and the formation of compact objects. Key milestones in the history of HMXBs include [1]:

- *Early discoveries: birth of X-ray astronomy (1960s).* The field began in 1962 with the discovery of the first extrasolar X-ray source, Sco X-1 [2]. A few years later, Centaurus X-3 (Cen X-3) was discovered, first as an X-ray source [3] and then as an X-ray pulsar [4]. Early observations were limited by poor angular and spectral resolution, and the physical origin of X-ray emission was debated. Accretion onto compact objects

Table 1. List of BeXBs with confirmed optical counterparts.

Source Name	Spectral Type	*V*-Band (mag)	P_{spin} (s)	P_{orb} (days)	e	Distance (kpc) Gaia DR3	$-$EW(Hα) (Å)
4U 0115+63	B0.2Ve	15.4	3.6	24.3	0.34	$5.7^{+0.5}_{-0.4}$	17 ± 2
IGR J01363+6610	B1IV-Ve	13.3	–	–	–	5.6 ± 0.4	72 ± 3
RX J0146.9+6121	B1Ve	11.3	1400	330 [††]	–	2.8 ± 0.2	17 ± 1
IGR J01583+6713	B2IVe	14.4	–	–	–	$5.6^{+0.6}_{-0.4}$	75 ± 3
RX J0240.4+6112	B0Ve	10.8	–	26.5	0.54	2.50 ± 0.07	17 ± 1
Swift J0243.6+6124	O9.5Ve	12.8	9.9	27.6	0.10	$5.2^{+0.3}_{-0.2}$	11 ± 1
V 0332+53	O8–9Ve	15.4	4.4	33.8	0.37	5.9 ± 0.4	8.5 ± 0.5
X Per	B0Ve	6.1	838	250	0.11	$0.60^{+0.02}_{-0.01}$	40 ± 2
RX J0440.9+4431	B0.2Ve	10.7	202.5	150	–	$2.44^{+0.08}_{-0.09}$	13.5 ± 0.5
1A 0535+262	O9.7IIIe	9.2	105	111	0.47	1.77 ± 0.06	24 ± 1
IGR J06074+2205	B0.5Ve	12.2	373.2	80 [†]	–	$6.0^{+0.9}_{-0.6}$	12 ± 1
MXB 0656–072	O9.5Ve	12.3	160.4	101.2	0.4 [††]	5.7 ± 0.5	25 ± 2
MAXI J0655–013	O9.5-B0Ve	11.7	1130	27.9	0.48	$3.7^{+0.9}_{-0.6}$	33 ± 3
4U 0728–25	O8–9Ve	11.3	103.3	34.5	–	6.7 ± 2.3	9 ± 1
2SXPS J075542.5–293353	B0Ve	10.2	307.8	59.7	0.06	3.3 ± 0.2	23 ± 2
RX J0812.4–3114	B0.2IVe	12.7	31.9	80	–	$6.7^{+0.5}_{-0.4}$	20 ± 1
GS 0834–430	B0–2III-Ve	20.4	12.3	105.8	0.15	$5.7^{+2.4}_{-1.6}$	32 ± 2
MAXI J0903–531	B1.5–2III-Ve	13.3	14.05	57.0	–	$9.2^{+3.3}_{-3.8}$	4.5 ± 0.5
GRO J1008–57	B1Ve	15.3	93.5	249.5	0.68	3.5 ± 0.2	29 ± 1
RX J1037.5–5647	B0III-Ve	11.5	860	61	–	5.1 ± 0.4	1.5 ± 0.5
1A 1118–616	O9.5IV-Ve	12.1	406.5	24	< 0.1	$2.90^{+0.09}_{-0.08}$	90 ± 10
IGR J11435–6109	B0.5Ve	16.4	161.8	52.4	–	$7.7^{+1.7}_{-1.9}$	26 ± 2
4U 1145–61	B0.2IIIe	9.0	292	186.5	> 0.5	$2.06^{+0.08}_{-0.09}$	45 ± 3
4U 1258–61(GX 304–1)	B2III-Ve	14.4	272	132.5	0.5	1.90 ± 0.05	39 ± 2
2S 1417–624	B1Ve	16.9	17.7	42.12	0.45	$6.4^{+3.6}_{-2.1}$	12 ± 2
Swift J1626.6-5156	B0Ve	15.5	15.4	132.9	0.08	$7.9^{+4.1}_{-2.0}$	40 ± 2
XTE J1946+274	B0–1V-IVe	16.6	15.8	172	0.25	$12.1^{+2.6}_{-2.2}$	52 ± 4
KS 1947+300	B0Ve	14.5	18.7	40.4	0.03	14^{+3}_{-2}	19 ± 1
Swift J2000.6+3210	B0–2Ve	16.2	890	–	–	$8.4^{+1.8}_{-1.2}$	15 ± 2
EXO 2030+375	B0Ve	19.5	42	46.02	0.41	$2.4^{+0.5}_{-0.4}$	21 ± 2
GRO J2058+42	O9.5-B0IV-Ve	14.9	192	55	–	$8.9^{+0.7}_{-0.8}$	15 ± 1
SAX J2103.5+4545	B0Ve	13.9	358	12.7	0.40	$6.2^{+0.4}_{-0.5}$	5.5 ± 0.5
IGR J21343+4738	B1IVe	14.1	320	–	–	$8.5^{+1.1}_{-0.8}$	15 ± 5
Cep X–4	B1–2Ve	14.3	66.3	–	–	$7.2^{+0.68}_{-0.6}$	55 ± 1
4U 2206+54	O9.5Ve	9.8	5550	19.2	0.15	$3.2^{+0.2}_{-0.1}$	5.0 ± 0.5
SAX J2239.3+6116	B0Ve	14.4	1247	263	–	$7.3^{+0.7}_{-0.5}$	19 ± 2
IGR J22534+6243	B1Ve	15.3	46.67	–	–	$8.9^{+1.4}_{-0.9}$	39 ± 1

Sources: [5–8], Simbad data base, and author's own search; [†] $P_{orb} = 80/n$, where $n = 2, 3, \ldots$; [††] Tentative.

emerged early as a viable mechanism, particularly within close binary systems, where mass transfer could efficiently power luminous X-ray emission [9].

- *Consolidation of the binary model (1970s).* During this decade, the binary nature of Galactic X-ray sources became widely accepted. Systems were classified based on the nature of the compact object (white dwarf, neutron star, or black hole) and the mass of the donor star, leading to the distinction between low-mass and high-mass X-ray binaries [10,11]. Among HMXBs, two main subclasses were recognized: systems with supergiant donors and those with Be-type companions [12]. A major breakthrough was the discovery of coherent X-ray pulsations and cyclotron resonance scattering features [13,14], establishing that most HMXBs host strongly magnetized neutron stars with field strengths of $(1-10)\times 10^{12}$ G.
- *Mass transfer and phenomenology (1980s).* By the 1980s, SGXBs were understood as persistent sources powered mainly by wind accretion from luminous supergiants, whereas BeXBs were recognized as transient systems associated with circumstellar decretion disks around Be stars [15,16]. Two types of BeXB X-ray outbursts were defined: periodic, orbitally modulated Type I outbursts near periastron, and rarer, brighter, irregular Type II outbursts linked to large-scale disk disturbances [17]. The realization that distinct HMXB subclasses correspond to different mass-transfer mechanisms culminated in the Corbet diagram, which revealed a correlation between neutron-star spin period and orbital period and provided a unifying framework for HMXB taxonomy [18].
- *Expansion of the BeXB picture (1990s).* Improved X-ray sensitivity led to the discovery of persistent, low-luminosity BeXBs [19]. These systems differ from classical transient BeXBs by exhibiting long spin periods, weak variability, low accretion rates, and likely wide, nearly circular orbits, indicating steady accretion from the tenuous outer regions of Be-star disks rather than episodic disk-neutron star interactions.
- *New subclasses and complexity (2000s).* The launch of the INTEGRAL mission marked a turning point, by revealing previously hidden populations of SGXBs and introducing new subclasses. Supergiant Fast X-ray Transients were identified as systems with supergiant donors that exhibit brief, intense X-ray flares separated by long periods of quiescence [20], challenging the earlier assumption that all SGXBs are persistent emitters. This decade also saw the recognition of γ Cas analogues—Be stars with anomalously hard, thermal X-ray emission at relatively low luminosities and lacking detected pulsations, suggesting fundamentally different emission mechanisms, possibly involving magnetic star-disk interactions or accretion in unusual regimes [21].
- *Recent developments (2010s).* The diversity of HMXBs expanded further with the identification of γ-ray binaries, systems emitting primarily above MeV energies, likely powered by the interaction between a pulsar wind and the massive companion winds [22]. Another major discovery was the first Be-star binary hosting a black hole, enriching BeXB phenomenology though its nature remains under debate [23,24].

3. Variability Timescales

Variability in a system generally means that some quantity or observable changes over time. The timescales of this variability help identify the physical processes involved and their origins. Variability can be periodic, quasi-periodic, or aperiodic. Be/X-ray binaries exhibit variability across all timescales, from seconds to years, and across many different bands of the electromagnetic spectrum.

In the X-ray band, variability originates from accretion. Timescales related to accretion range from fractions of a second to hours, appearing as pulsations, quasi-periodic oscillations, and broadband noise in power spectra [25–27]. Longer timescales (weeks to months)

show up as orbitally modulated Type I X-ray outbursts. The slowest variability, on scales of years, is linked to mass transfer between the Be star and neutron star, manifesting as unpredictable giant or Type II X-ray outbursts.

In the optical band, short-term variations (hours) are connected to the Be star's atmosphere and its rapid rotation. Intermediate timescales (weeks to months) relate to processes in well-developed circumstellar disks, such as the precession of density perturbations. The longest timescales (years) correspond to the formation, growth, and dissipation of these disks.

The physical information extracted from variability studies naturally depends on the observable under investigation. For long-term monitoring, easy-to-measure observables are preferred: the Hα emission line in optical spectra is particularly powerful for diagnosing the size, density, and structure of Be star decretion disks because it forms over much of the disk and is optically thick. Its strength and shape (e.g., equivalent width, V/R ratios, peak separation) reveal disk density, radial extent, and velocity fields [28–31]. It is also less affected by interstellar extinction than some helium or metal lines. From photometry, magnitudes and colors are easily obtained. In polarimetry, the polarization angle and the degree of polarization, can be directly computed from aperture photometry.

The variability in BeXBs arises from three main sites: the Be star, the circumstellar disk, and the neutron star. The following review discusses key physical processes linked to different variability timescales according to their origin. Table 2 summarizes these timescales, their physical origins, and the processes they probe.

Table 2. Typical variability time scales in BeXBs.

Time Scale	Physical Process	Observational Evidence	Origin
Seconds	Accretion	Pulsations, QPO	Neutron star
Hours	Non-radial pulsations, Rotation	Line profile var. Multi-periodic lightcurves	Be star
Weeks to Months	Density perturbations, Orbital motion	V/R var. Brightness var. X-ray outbursts	Be disk Binary
Years	Disk formation and dissipation	Line profile var. Line strength var. Brightness var. Color changes	Be disk

4. The Be Star

The origin of the Be phenomenon, that is, the identification of the ultimate mechanism that leads to the formation of a circumstellar disk around the equator of a Be star is one of the major open questions in the field. Although there is general consensus that the disk formation is related to the high rotational velocity of the Be star, there is no agreement on how close to critical velocity (velocity at which centrifugal forces balance Newtonian gravity) they rotate. Rotation rates (rotation velocity normalized by the star's critical rotation speed) lie in the range 70–80% [32,33], 90% [34], or even higher [35]. Several scenarios have been put forward to explain these fast rotation rates [36]: (i) Be stars are born as fast rotators; (ii) the high rotation speeds result through accretion from a companion during an evolutionary phase as a binary system; (iii) they become fast rotators as they evolve along the main sequence. The rotation rate is a key ingredient in understanding the formation of the equatorial disk. The higher the rotation rate, the easier it is for gas to lift up and launch material into a ballistic orbit. Still, some other mechanism must be at play. The primary trigger for episodic mass ejection into a disk is non-radial pulsations (NRP).

Constructive interference or beating between two or more NRP modes may contribute to the sudden increases in pulsation amplitude and lead to a mass outburst [37,38].

Observationally, NRPs manifest as short-term (hours) variability. NRPs divide the stellar surface in regions with different temperatures and velocity fields. If the amplitude of the pulsations is large enough, the temperature variations across the surface of the star can be detected photometrically as differences in brightness [39–41], while the redistribution of flux over the absorption line profile as the star rotates creates moving patterns of peaks and troughs that can be detected spectroscopically [42–44].

NRPs are a very common, if not ubiquitous, feature intrinsic of BeXBs [45]. As in classical Be stars, BeXBs display frequency groups, long-term irregular variability, isolated signals, and light outbursts. This type of variability in BeXBs occurs mainly on timescales shorter than ∼12 h. The peaks of the period distribution correspond to modulations of 5–10 h, but there is also a significant contribution on timescales ∼1 day.

Figure 2 shows the *Transiting Exoplanet Survey Satellite* (TESS) light curve of 1A 0535+262 (top panel), the normalized light curve (middle panel), and the corresponding periodogram (bottom panel). The frequency analysis reveals the characteristic presence of two frequency groups, centered around 1 and 2 d^{-1}. Notably, the oscillation amplitude increases after each local minimum and then gradually decreases along the ascending branch toward the brightness maxima. Following each maximum, the amplitude reaches its lowest values. This behavior is consistent with the general trend observed in classical Be stars, in which an increase in the mean stellar brightness is associated with the enhancement of the amplitude of one or more pulsation frequency groups, which in turn, are identified with mass ejection episodes [46].

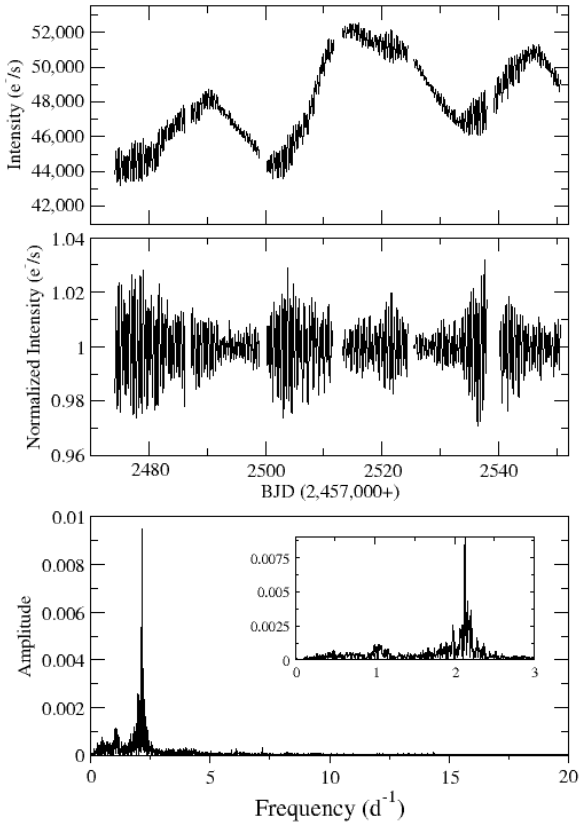

Figure 2. (**Top panel**): TESS light curve of 1A 0535+26. (**Middle panel**): normalized light curve. (**Bottom panel**): periodogram. Note the largest amplitude of the oscillation during the brightening parts of the light curve. Adapted from [45].

An alternative mechanism (or in addition to NRPs) that may eject material from the photosphere to form the disk is magnetic reconnection associated with localized magnetic fields generated by convection [41].

5. The Decretion Disk

As explained in the previous section, the decretion disk forms when material is ejected from the stellar photosphere due to mechanisms such as fast rotation, non-radial pulsations, or magnetic reconnection. What happens to the material after it is ejected remains an open question, although significant theoretical progress has been made in recent years [47–49]. Observationally, changes related to disk evolution are evident in the optical/IR and X-ray bands. Photometrically, the contribution of the disk to the overall brightness increases at longer wavelengths, producing an infrared excess and reddening colors as the disk develops [50]. Spectroscopically, hydrogen emission lines, particularly Hα, show significant variations in profile and strength, reflecting structural changes in the disk [51]. Polarimetrically, Thomson scattering produces continuum polarization that traces disk's density and orientation changes [52]. Disk size and density determine how much material the neutron star can accrete, thereby regulating the occurrence of X-ray outbursts.

5.1. Disk Truncation

Disks in BeXBs are smaller and denser than those around isolated Be stars. This is because the neutron star's tidal forces truncate the disk. Both observations [51,53] and the-

ory [54–56] support disk truncation in BeXBs. The truncation radius, defined as the distance where tidal and viscous forces balance, depends on disk parameters such as kinematic viscosity (which measures internal friction) and aspect ratio (the disk's thickness relative to its radius), as well as binary parameters including orbital period and eccentricity [47,48,54,57].

The first observational evidence for truncation came from the correlation between the equivalent width of the Hα line and the orbital period [51,53]. Systems with narrow orbits experience stronger tidal forces from the neutron star. As a result, their disks cannot maintain a stable configuration over long timescales. In contrast, systems where the neutron star orbits farther away (long orbital periods) allow the disk to develop more freely. Because the Hα equivalent width measures the disk's extent [30,31], this correlation implies that wider-orbit systems develop larger and more stable disks. Figure 3 shows an updated version of the $EW(H\alpha)$-$P_{\rm orb}$ diagram for Galactic BeXBs. The system with the longest orbital period shown in Figure 3 (left panel) that lies outside the general trend is GRO J1008–57, which has the most eccentric orbit ($e = 0.7$). Although orbital period is easier to determine observationally, the truncation radius is expected to be determined by the periastron distance, which for highly eccentric orbits would be comparable to systems with shorter orbital periods. The right panel in Figure 3 shows the relationship between Hα equivalent width and periastron distance. GRO J1008–57 with $\sim$142 $R_\odot$ lies confortable in the middle of the correlation.

Polarization studies further support the idea that BeXBs have denser, truncated disks compared to classical Be stars. On average, BeXBs exhibit higher intrinsic polarization than isolated Be stars [52]. Since polarization degree reflects the number of scattering electrons, models predict that polarization increases with disk density due to more electrons available for Thomson scattering [58]. Figure 4 compares the normalized distribution of intrinsic polarization degrees for classical Be stars (spectral types O9–B2) and BeXBs. The normalized histogram is computed so that the total area under the histogram equals 1, i.e., it represents an estimate of a probability density function: $p(x_i) \approx \frac{n_i}{N\Delta x}$, where n_i is the number of measurements in bin i, Δx is the bin width, and N the total number of measurements. Here $N = 314$ for Be stars, $N = 11$ for BeXB, and Δx = 0.4. The data are from [59] (Be stars) and [52] (BeXBs). Be stars generally show lower polarization; notably, only five stars in the [59] sample had polarization degrees above 2%, all within the B0–B2 spectral range. In contrast, about half of the BeXB sample displayed maximum intrinsic polarization degrees above 2%. Moreover, Figure 4 shows that systems with longer orbital periods tend to have higher polarization fractions, reinforcing the idea that the neutron star limits the disk's free expansion.

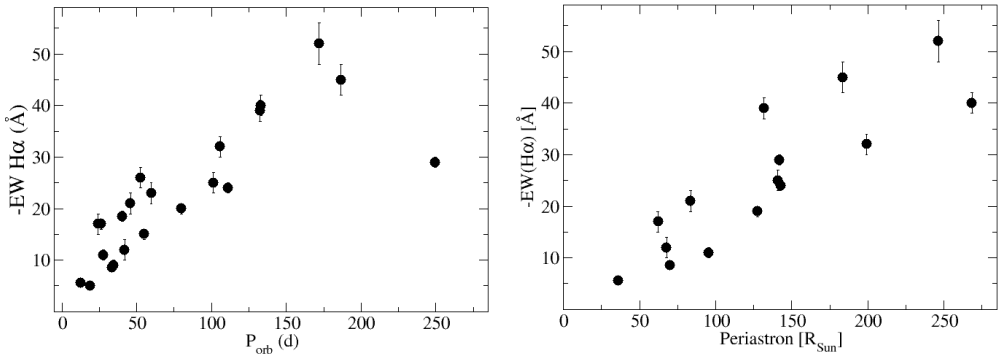

Figure 3. Hα equivalent width as a function of the orbital period (**left**) and periastron distance (**right**).

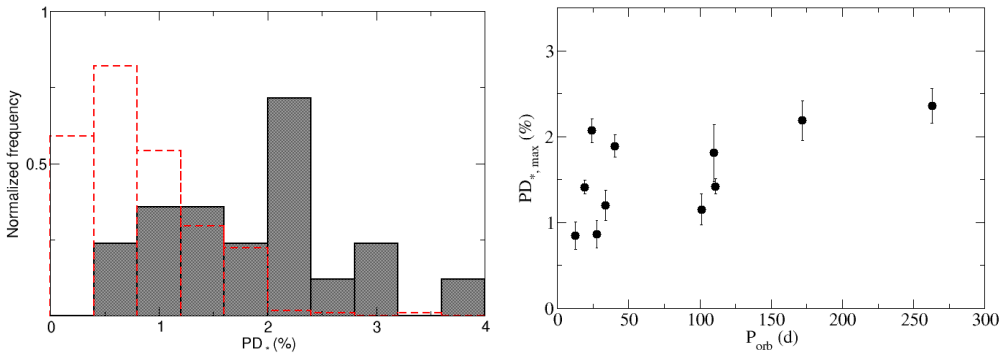

Figure 4. (**Left**): Normalized distribution of the intrinsic polarization degree of classical Be stars (red dashed line) and BeXBs (black shaded rectangles). (**Right**): Intrinsic polarization degree as a function of the orbital period. Adapted from [52].

5.2. Disk Formation and Dissipation Cycles

The disk evolves on timescales of years, undergoing formation and dissipation phases that control both long-term optical/infrared variability and X-ray activity through mass supply for accretion.

Figure 5 displays the evolution of the Hα equivalent width (EW(Hα)) for several BeXBs, ordered in increasing value of the orbital period. This plot has an enormous diagnostic power as it covers the formation, growth, and dissipation of the decretion disk. The optical emission lines in Be stars, most prominently the Hα line, are formed through recombination within the dense, ionized gas of the circumstellar decretion disk, where intense ultraviolet radiation from the central B star ionizes hydrogen atoms, and the subsequent recombination of electrons with protons produces line emission. Consequently, EW(Hα) serves as a robust proxy for the presence or absence of the disk. Moreover, the size of the disk is directly related with the strength of the Hα line. This has been made evident through interferometric observations that have resolved the disk and enabled the measurement of the angular dimensions of Be star disks [28,30,31]. By convention, EW(Hα) is negative for emission lines and positive for absorption lines.

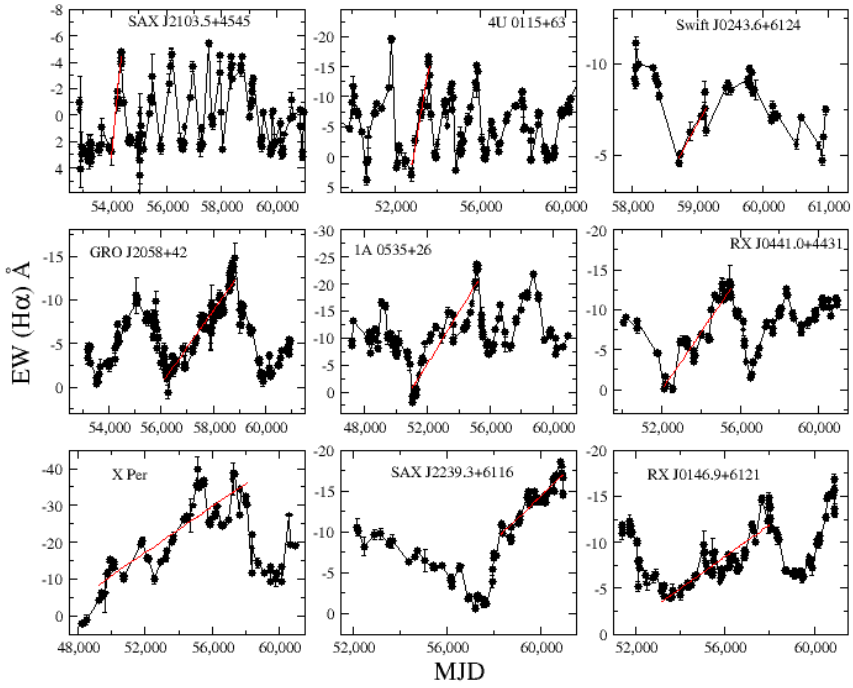

Figure 5. Evolution of the EW(Hα). The red lines represent a linear fit to the data points that correspond to the formation of the circumstellar disk after a low-optical state.

The timescale for a whole cycle is given in Table 3. There is a trend for longer formation-dissipation timescales in systems with longer orbital periods. A correlation between the orbital period and the so-called superorbital periods has been reported in many different types of X-ray binaries, although the physical mechanism behind the superorbital modulation differs [60]. In BeXBs, the superorbital modulation is driven by long-term evolution of the Be star's decretion disk, making this variability quasi-periodic rather than strictly coherent.

Table 3. Decretion disk formation and dissipation timescales in BeXBs.

Source	$P_{\mathbf{orb}}$ **(d)**	$P_{\mathbf{cycle}}$ **(d)**
SAX J2103.5+4545	12.7	600
4U 0115+63	24.3	1000
IGR J06074+2205	80 †	800
GRO J2058+42	55	3200
1A 0535+262	110	1700
RX J0441.0+4431	150	3500
RX J0146.9+6121	330 ††	3000

† $P_{\rm orb} = 80/n$, where $n = 2, 3, \ldots$; †† Tentative.

5.2.1. Disk-Loss Episodes

Although the disk is central to understanding the observed variability of BeXBs across multiple wavelengths, disk-loss events provide a unique opportunity to disentangle the intrinsic stellar emission from disk-related contributions, enabling a more reliable determination of the Be star's fundamental parameters. Similarly, the total reddening and polarization measured during a disk-loss episode should correspond entirely to the interstellar medium. Disk-loss episodes are best identified from spectroscopic observations when the Hα line profile reverts from emission into absorption, or equivalently, when the

EW(Hα) changes from negative to positive in Figure 5. Therefore, disk-loss episodes can be easily identified in Figure 5 by looking at epochs when EW(Hα) > 0.

5.2.2. Disk Growth

Figure 5 can also be used to estimate the disk growth rate, $d(EW(H\alpha))/dt = E\dot{W}(\mathrm{H}\alpha)$, following an optically faint (low) state: systems with shorter orbital periods exhibit faster growth rates. This correlation is further illustrated in Figure 6, which plots the growth rate as a function of orbital period. Since the mass ejection mechanism originates in the Be star and all BeXBs host spectrally similar companions (with optical counterparts ranging from O9 to B2), the observed correlation cannot be attributed to differences in mass ejection mechanisms, which would lack a plausible physical explanation. Instead, the trend is naturally explained by the tidal torque exerted by the neutron star, which drives an accumulation effect wherein material builds up in the inner disk. In wider-orbit systems, the neutron star's weaker tidal influence allows the disk to extend farther, resulting in a more gradual radial decline in surface density. By contrast, in close-orbit systems, the neutron star's proximity truncates the disk more severely, producing a steeper density gradient.

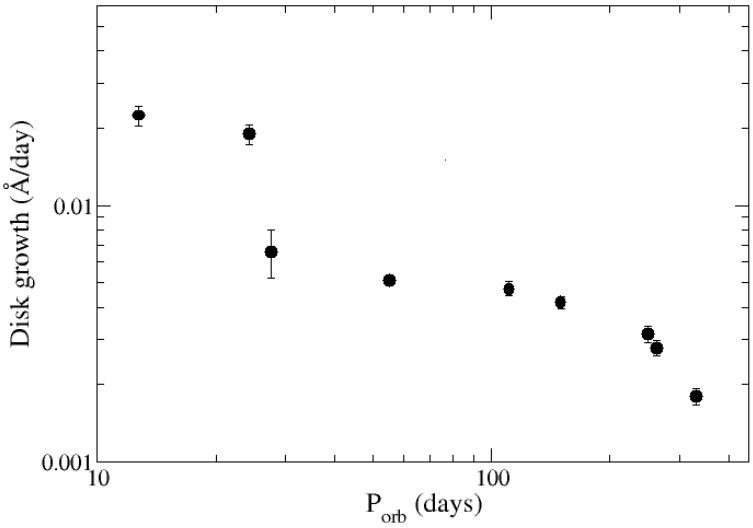

Figure 6. Disk growth rate after a disk-loss episode as a function of orbital period.

Two types of correlations between photometric magnitudes and color indices are observed during the formation and growth of the circumstellar disk, as traced, for example, by increasing Hα emission strength. The most common behaviour is a positive correlation, in which the brightness of the star (e.g., in the V band) increases simultaneously with the color index (e.g., B-V). In other words, as the disk reforms and grows, the system becomes both brighter and redder. A smaller number of stars exhibit a negative correlation. In these systems, stronger Hα emission is associated with a decrease in optical brightness. The fading observed in the V band is again accompanied by a reddening of the (B-V) color index. These correlations are generally interpreted as a geometrical effect [61]. Stars observed at very high inclination angles tend to display the inverse (negative) correlation, whereas systems viewed at inclination angles below a critical value, $i < i_{\mathrm{crit}}$, show the positive correlation. In nearly equator-on systems, the inner regions of the circumstellar disk partially obscure the stellar photosphere. At the same time, the small projected area of the disk on the plane of the sky minimizes its contribution to the observed continuum emission. As a result, the system becomes fainter as the disk grows. In contrast, for low- and intermediate-inclination systems, the disk contributes additional continuum emission

and effectively increases the apparent radiating area of the star-disk system. Consequently, disk growth is accompanied by an overall increase in brightness. Although the value of the critical inclination angle remains uncertain, available observations suggest a representative value of $i_{crit} \approx 75°$. This interpretation is supported by the larger number of systems that show a positive correlation than negative, the fact that the same star always show the same type of correlation, and also the fact that when spectra are available, negative correlations are related to stars that show shell spectra (a shell line is a spectral line that shows a narrow absorption component superimposed on the broader stellar emission profile and occurs when the Be disk is viewed at high inclination [62]). Figure 7 shows two examples of the evolution of brightness and color as the disk develops. GRO J2058+42 follows the more general case of increasing brightness and reddening as the disk grows (i.e., as EW(Hα) increases), corresponding to a low- or intermediate-inclination system. On the other hand, IGR J21343+4738 shows an overall drop in brightness as the disk grows, expected from a high-inclination system.

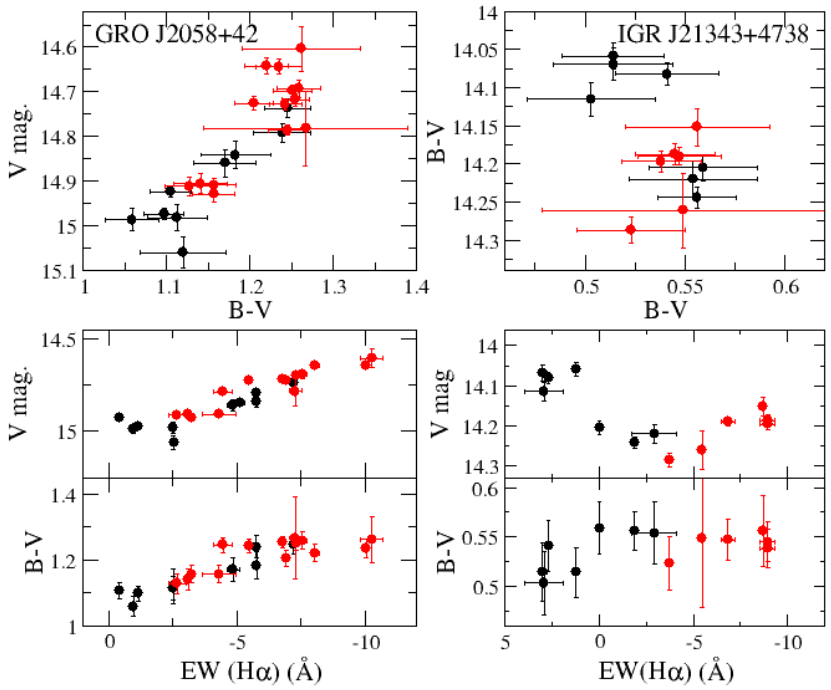

Figure 7. Evolution of the V magnitude and (B-V) color during the growth of the disk after a low-optical state. Different color data points refer to two different epochs of disk growth: black points correspond to observations in the interval 2005–2009 (GRO J2058+42) and 2009–2014 (IGR J21343+4738); red points correspond to the interval 2013–2019 (GRO J2058+42) and 2017–2020 (IGR J21343+4738).

5.2.3. Disk Formation and Dissipation: Predicting the Orbital Period of the System

If the observations encompass multiple cycles of disk formation and dissipation, the evolution of the EW(Hα) could, in principle, be used to estimate the orbital period of systems lacking an orbital solution. This estimation is based on the information presented in Figure 5 and the relationships involving the orbital period, specifically the EW_{max}(Hα)–P_{orb} diagram and the $\dot{EW}$(Hα)–P_{orb} relation. The results derived from these diagrams can then be cross-checked for consistency using the less constrained P_{cyc}–Porb diagram and the PD_{max}–P_{orb} diagram.

A notable feature of the data in Figure 5 is the increasing smoothness of the curves with longer orbital periods. Systems with shorter orbital periods show many more disk

formation and dissipation cycles, resulting in more "choppy" curves, whereas systems with longer orbital periods exhibit smoother evolutionary trends.

To illustrate this method, we consider two cases: IGR J06074+2205 and IGR J21343+4738. An orbital period of 80 days has been proposed for IGR J06074+2205 based on the occurrence of relatively weak type I X-ray outbursts. However, submultiples of this value could also be plausible, that is, $80/n$, where $n = 2, 3, \ldots$ [63]. The orbital period of IGR J21343+4738 remains unknown. Figure 8 shows the evolution of EW(Hα) for these two sources. From this figure we can extract the following information:

- IGR J06074+2205: $EW_{\rm max}$(Hα) = -12.5 Å, $E\dot{W}$(Hα) $\approx 0.017 \pm 0.003$ Å/day, $P_{\rm cyc} \approx$ 800 days. Also we know that $PD_{\rm max} = 1.7\%$
- IGR J21343+4738: $EW_{\rm max}$(Hα) = -20 Å, $E\dot{W}$(Hα) $\approx 0.007 \pm 0.001$ Å/day, $P_{\rm cyc} \approx$ 2400 days. Also, we know that $PD_{\rm max} = 0.8\%$

Using $EW_{\rm max}$(Hα) and $E\dot{W}$(Hα) and the best-fit in Figures 3 and 6, we estimate the orbital period of IGR J06074+2205 to be 18–30 days and predict that the orbital period of IGR J21343+4738 should fall in the range 58–72 days. Figure 9 shows the position of these two sources in the various diagrams.

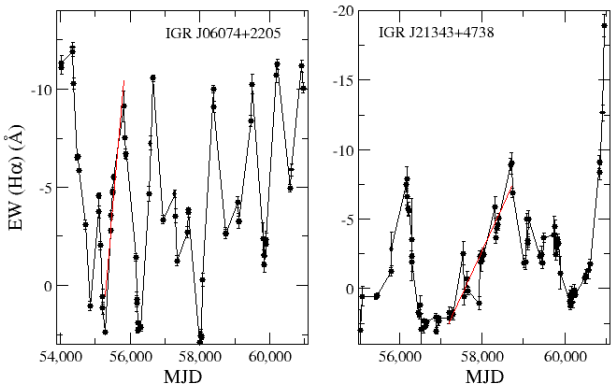

Figure 8. Evolution of the EW(Hα) for IGR J06074+2205 and IGR J21343+4738. The red lines represent a linear fit to the data points that correspond to the formation of the circumstellar disk after a low-optical state.

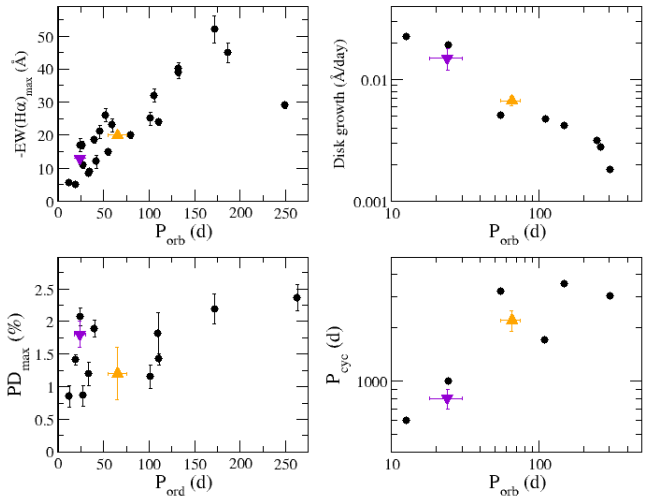

Figure 9. Various observable as a function of orbital period. The colored points correspond to IGR J06074+2205 (violet) and IGR J21343+4738 (orange).

6. The Neutron Star

BeXBs host a strongly magnetized neutron star with magnetic fields in the order of 10^{12}–10^{13} G. Information about the magnetic field strength is obtained from the detection of cyclotron resonant scattering features (CRSF) [64]. The magnetic field is also responsible for the X-ray pulsations. Pulsations result from the misalignment of the neutron star's rotational axis and the magnetic axis [13].

6.1. X-Ray Periodic, Quasi-periodic, and Aperiodic Variability

Transient BeXBs exhibit strong X-ray variability. Timescales attributed to the accretion process range from a fraction of a second to hours, resulting in pulsations, quasi-periodic oscillations (QPOs) in the millihertz range, and band-limited noise in the power spectrum [25–27].

Periodic variability arises from the rotation of the neutron star and is observed as coherent X-ray pulsations in the light curves. The accretion flow is funneled by the strong magnetic field onto the magnetic polar caps, where it impacts the stellar surface and forms localized hot spots. In these regions, the kinetic energy of the infalling material is efficiently converted into X-ray radiation through shock heating and subsequent radiative processes. If the magnetic axis is inclined relative to the rotation axis, the hot spots sweep across the observer's line of sight as the star spins, producing the observed pulsations. The corresponding spin periods typically range from about 1 to 1000 s. Variations in the spin period allow estimation of the magnetic field strength and can be used to derive orbital solutions. Short-term changes in pulse period, measured as delays in pulse arrival times caused by the Doppler effect from orbital motion, help determine the orbital parameters of the binary system [65]. Long-term changes in the pulse period are linked to the exchange of angular momentum between the accretion flow and the neutron star. These secular spin-up or spin-down trends provide valuable constraints on the neutron star's magnetic field strength and on the physical properties and geometry of the accretion flow [66].

QPOs are associated with inhomogeneities in the accretion flow or plasma instabilities generated around the magnetospheric boundary [27]. Two models have been put forward to explain QPOs in accreting pulsars: the Magnetospheric Beat-Frequency Model (BFM) [67] and the Keplerian Fequency Model (KFM) [68]. The difference between the two is that the BFM proposes that the QPO frequency is the beat between the neutron star's

spin frequency and the Keplerian frequency of matter at the inner edge of the accretion disk, while the KFM suggests that the QPO frequency is directly equal to the Keplerian orbital frequency at the inner disk. Thus, in the BFM $\nu_{\rm QPO} = \nu_{\rm K} - \nu_{\rm NS}$, while in the KFM $\nu_{\rm QPO} = \nu_{\rm K}$. Assuming the radius of the inner accretion disk scales by the accretion rate (and hence the X-ray luminosity), the Keplerian frequency of the inner accretion disk, and thereby the QPO frequency, is expected to increase with luminosity in both KFM and BFM, as observed [69]. A third model, the magnetic disk precession model [70], attributes mHz QPOs to warping/precession modes induced by magnetic torques near the inner edge of the accretion disk. None of the three models can explain the origin of QPOs in all the systems. For example, the identification of the QPO frequency with the Keplerian frequency associated with the disk magnetosphere boundary in the KFM imposes the condition $\nu_{\rm NS} < \nu_{\rm QPO}$, which is not always met.

Aperiodic variability appears as band-limited noise, whose power typically decreases as the frequency increases. This noise is modeled by fitting the power density spectra (PSD) with combinations of several Lorentzian [71,72] and/or (broken) power-law functions [73,75]. Accreting pulsars, hence BeXBs, generally display breaks in their PDS. Ref. [25] proposed that the break frequency is directly related to the inner edge of the disk, specifically at the interface between the accretion disk and the magnetosphere. Interestingly, at low flux, the noise power breaks occur near the pulse frequency, indicating corotation between the neutron star and the accretion disk. As the X-ray luminosity increases, the break frequency increases. This correlation supports the disk-magnetosphere origin of the frequency. Fluctuations of the X-ray flux are largely caused by fluctuations of the mass accretion rate onto the neutron star surface. An increase in the mass accretion rate decreases the size of the magnetosphere (and hence the inner radius of the disk), so that the characteristic frequency at the inner edge of the disk/flow increases, and the inner parts of the accretion disks rotate much faster than the central object. This correlation between the break frequency and X-ray flux has been observed in many sources [71–75]. Some examples are shown in Figure 10.

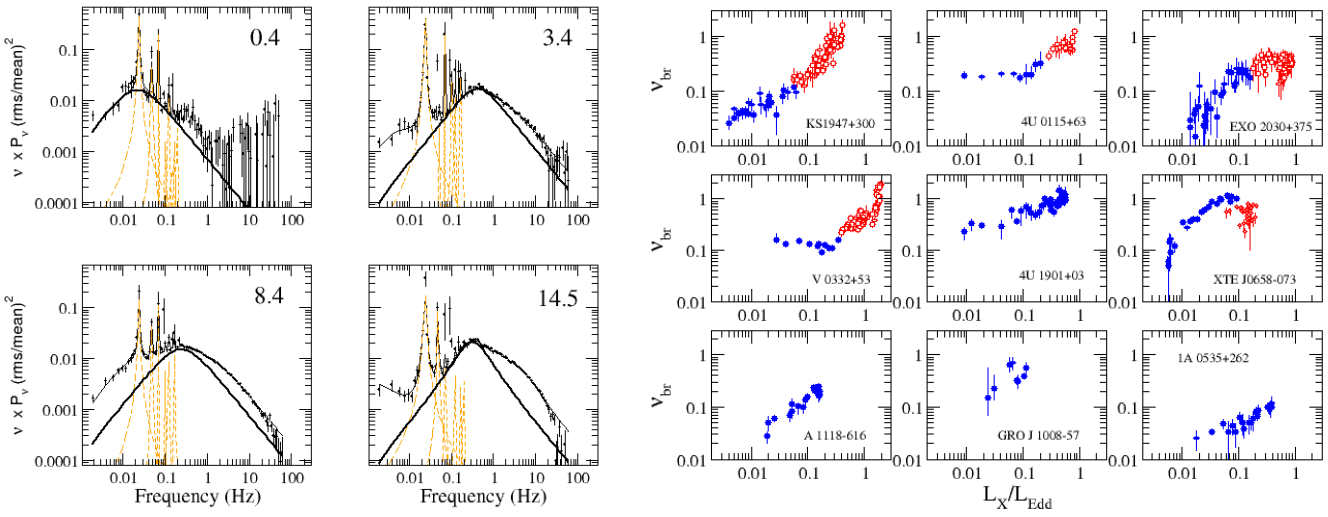

Figure 10. (**Left**): Power spectrum of EXO 2030+375 at different X-ray luminosity (given at the top right of each panel in units of 10^{37} erg s^{-1}. Orange lines represent fits to the coherent pulsation and its harmonics, while the black line corresponds to the main broad-band noise component. Adapted from [71]. (**Right**): Break frequency versus X-ray luminosity for various BeXBs. Blue and red circles correspond to the HB and DB, respectively (see Section 6.4 for an explanation of these two states).

6.2. X-Ray Outbursts

The vast majority of BeXBs are hard X-ray transients that shine bright during X-ray outbursts, which are traditionally divided into two types [76]:

- Type I (or normal) outbursts are relatively regular and often quasi-periodic events, typically peaking near periastron passage of the neutron star. They reach moderate X-ray luminosities, ($L_X \lesssim 10^{37}$ erg s^{-1}), and usually last for a limited fraction of the orbital period (∼0.2–0.5 (P_{orb})). These events are generally interpreted as enhanced accretion episodes occurring when the neutron star interacts with the outer regions of the Be star's circumstellar disk.
- Type II (or giant) outbursts are substantially brighter, with luminosities approaching or reaching the Eddington limit for a neutron star, ($L_X \sim 10^{38}$ erg s^{-1}). Unlike type I events, they show no preferred orbital phase and may persist for a large fraction of an orbital cycle or even several orbital periods. They are commonly associated with the accretion of a significant portion of the Be disk. Current models attribute these events to major structural changes in the circumstellar disc, such as warping and the development of eccentricity in a highly misaligned disc, which enable enhanced mass transfer onto the neutron star [77,78].

Figure 11 shows representative examples of these two type of X-ray outbursts. It is not uncommon to observe a series of type I outbursts following a major type II event.

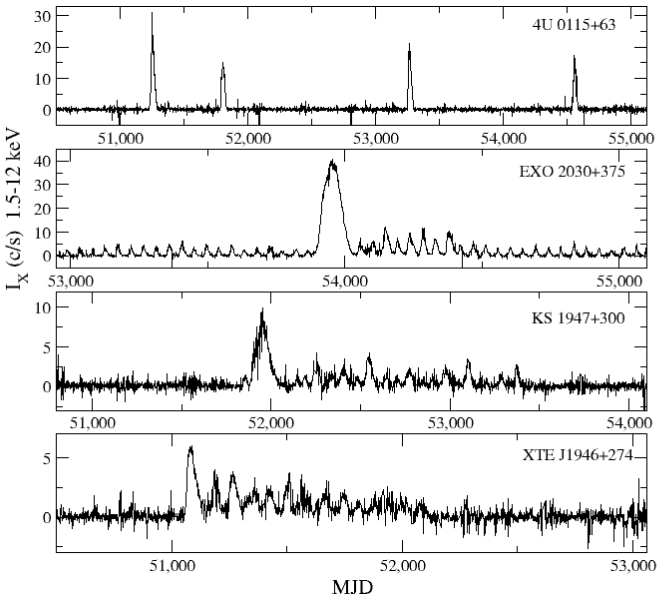

Figure 11. The two types of X-ray outbursts in BeXBs: low intensity, orbitally modulated, and shorter duration outbursts (type I) and giant and longer outbursts (type II). In this figure, 4U 0115+63 displays only type II outbursts, whereas KS 1947+300 and XTE J1946+274 show a type II outburst followed by a series of type I outbursts. EXO 2030+375 exhibits type I outbursts before and after a type II outburst. The X-ray data were obtained with the RXTE/ASM All Sky Monitor.

6.3. Disk–Neutron Star interaction

Although it is commonly understood that the outbursts are caused by mass transfer from the Be disk to the neutron star, the detailed mechanism remains uncertain. In particular, the connection between the Be disk and the resulting X-ray activity is still debated. Type II outbursts are observed in systems with both large and small disks. Furthermore, some systems with large disks exhibit no X-ray activity [79]. Since the disk is truncated, significant accretion can only occur if the disk becomes sufficiently asymmetric and dense to overflow the truncation radius. The prevailing hypothesis is that giant outbursts happen

when the neutron star captures a large amount of gas from a warped, highly misaligned, and eccentric Be disk. Models indicate that such highly distorted disks lead to enhanced mass accretion when the neutron star passes through the warped region [77,78].

A mechanism proposed for the occurrence of type II outbursts in BeXBs is the Kozai–Lidov (KL) mechanism [80,81]. The key idea in this mechanism is that the product of the disk's inclination and eccentricity remains constant. Thus, a test particle that is initially on a circular orbit in a misaligned disk undergoes a series of oscillations where the inclination and eccentricity interchange periodically. The eccentricity growth causes the disk to overflow its Roche lobe and transfer material to the companion neutron star [82,83].

Since the disk serves as the reservoir of material available for accretion, a decrease in the size of the Be star disk should be observed following a major outburst. Indeed, observations confirm the dissipation of the disk; however, the extent of this loss, ranging from complete destruction to a minor reduction, depends on the geometry and parameters of the orbit. Figure 12 shows representative examples of the connection between X-ray outbursts and the EW(Hα). A substantial decrease in EW(Hα) (hence in the extent of the disk) is apparent after major X-ray outbursts.

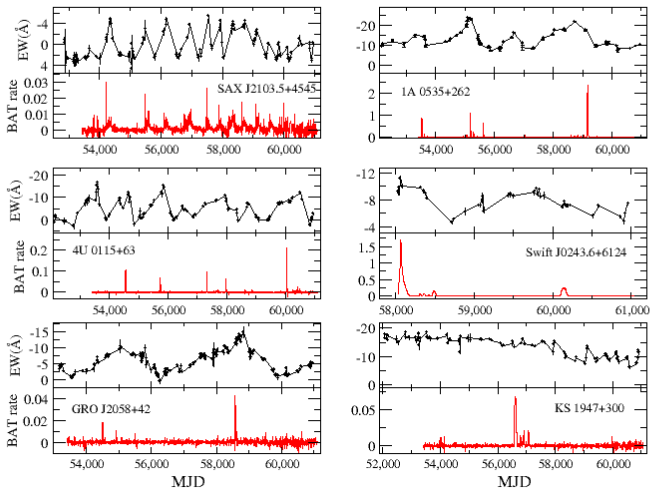

Figure 12. Optical (black) and X-ray (red) variability. After major X-ray outbursts the Be star's disk weakens. The X-ray data were obtained with the Swift/BAT Hard X-ray Transient Monitor.

6.4. Accretion Regimes

Most of the time, BeXBs are in a dormant or quiescent X-ray state and become detectable only during outburst. Centrally important to their behavior, the disk acts as the primary reservoir of matter for accretion onto a compact object, meaning its presence directly dictates X-ray variability and outbursts. If the disk dissipates completely, mass transfer to the companion star halts and X-ray emission should cease. However, at least three systems have shown X-ray emission during disk-loss phases: 1A 0535+262 [84], IGR J21343+4738 [85], and SAX J2103.5+4545 [86]. In addition, many more sources have been detected in a quiescent state at luminosities $L_X \lesssim 10^{34}$ erg s^{-1} [87]. The origin of the quiescent X-ray emission remains unclear. Two basic mechanisms have been proposed to explain X-ray emission from accreting pulsars at very low luminosities: accretion and cooling of the neutron star surface. Each mechanism implies different physical conditions. Accretion may occur at the magnetosphere via a stellar wind or through an accretion disk. Cooling may originate from the entire neutron star surface or from the polar caps. Timing and spectral analyses can help distinguish between these scenarios. In general, accretion leads to a

power-law dominated X-ray spectrum (due to Comptonization) and significant variability (rms > 10%), while cooling produces a thermal spectrum and a white-noise-dominated power spectrum.

During Type II outbursts, the X-ray luminosity increases by several orders of magnitude. This dramatic increase is associated with fundamental changes in the accretion flow configuration. The neutron star's strong magnetic field disrupts the accretion flow at some distance from its surface and channels the matter onto the magnetic polar caps, creating hot spots and an accretion column. The conditions prevailing in the accretion column define two accretion regimes: super- and sub-critical. These two regimes differ in the way the radiation pressure of the emitting plasma is capable of decelerating the accretion flow. In the super-critical regime, at high luminosities, radiation pressure dominates, decelerating the accretion flow via photon interactions. A radiation-dominated shock halts the flow at some distance above the neutron star surface [88–90]. In the sub-critical regime, radiation pressure is insufficient to stop the flow, which continues to the surface, where it is decelerated by multiple Coulomb scatterings with thermal electrons and nuclear collisions with atmospheric protons [91,92]. The luminosity marking the transition between these regimes is known as the critical luminosity, $L_{\rm crit}$.

Observational evidence for this transition includes changes in pulse profiles and correlations between cyclotron line energy and luminosity. As X-ray luminosity increases during an outburst, the pulse profile typically changes from a single to a double peak, interpreted as a change in accretion column structure and the formation of a radiation shock. This corresponds to a change from a pencil beam (photons escaping along the magnetic field axis) to a fan beam (photons escaping sideways due to the shock) [93,94]. Because the cyclotron line energy is representative of the magnetic field strength at the location where the line is formed, we expect its energy to change with changes in the structure of the accretion column. A bimodal behavior has been observed. Some sources show a positive correlation between cyclotron energy and luminosity (indicative of the sub-critical regime), whereas others show an anticorrelation (indicative of the super-critical regime) [95,96].

Further evidence for the transition between accretion regimes comes from variability in the X-ray spectral continuum. The hardness–intensity diagram (HID) is a useful tool to describe the rich variability patterns during outbursts. The source traces different branches or states in this diagram as it progresses through an outburst. Two main branches are observed in BeXBs: the "horizontal" branch (HB), corresponding to the low-luminosity sub-critical state, and the "diagonal" branch (DB), associated with the high-luminosity super-critical state [72]. The luminosity at which the source transitions between these branches would naturally correspond to the critical luminosity. From a theoretical perspective, $L_{\rm crit}$ depends on many factors, including the neutron star's mass and radius, the size of the hot spots, magnetic field strength, temperature, photon energy, and polarization [89,95,96]. Generally, larger magnetic fields correspond to higher critical luminosities. Since different systems have different magnetic fields, the sub-critical to super-critical transition must occur at different luminosities, consistent with observations. Figure 13 shows examples of HIDs illustrating this behavior.

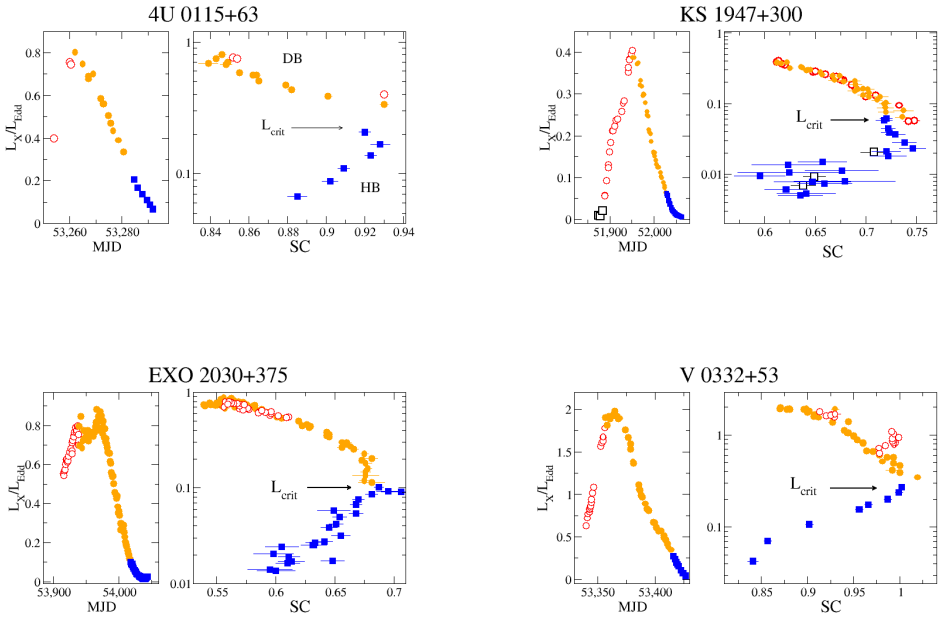

Figure 13. HID for four BeXBs during a type II outburst. Different colors represent different instances during the X-ray outbursts as indicated in the light curve (smaller panels) of each source. The soft colour (SC) is defined as the ratio 7–10 keV/4–7 keV. Typically, the Eddington luminosity for a neutron star is 1.7×10^{38} erg s^{-1}. The data were obtained with the RXTE/PCA instrument.

The typical energy spectral continuum of an accreting pulsar is well described by an absorbed power-law and exponential cutoff. The absorption at the lower energy end of the spectrum is caused by interstellar gas through the photoelectric effect. The power-law and exponential cut off at the higher energy of the spectrum is attributed to comptonization. Hardness ratios (HR) represent the simplest way to characterize the X-ray spectral continuum. Chosing them appropriately, the HR is a measure of the slope of the power law. However, a more accurate measure of the spectral continuun is provided by the photon index (i.e., the exponent of the power law). Similar to the HR, the photon index Γ also exhibit a break when plotted as a function of X-ray luminosity or flux [72,97,98], indicating a major change in the configuration of the accretion flow and/or the structure of the accretion column; i.e., it marks the transition between states (Figure 14).

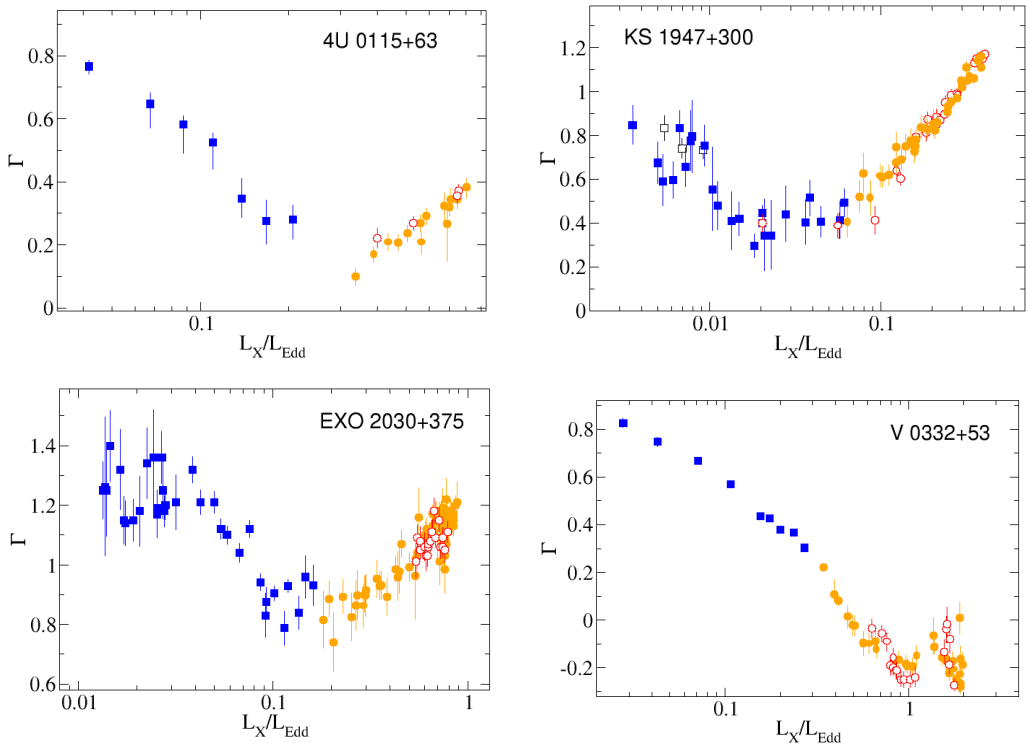

Figure 14. Photon index Γ as a function of X-ray luminosity. Symbols as in Figure 13.

7. Conclusions

Be/X-ray binaries constitute the largest and most diverse subgroup of neutron star high-mass X-ray binaries, serving as invaluable laboratories for the study of accretion physics, stellar evolution, and disk dynamics. Their hallmark feature, the decretion disk formed around the Be star, plays a crucial role in regulating the mass transfer to the neutron star and thereby dictates the rich variability observed across multiple wavelengths and timescales. The complex interplay between the Be star's rapid rotation, non-radial pulsations, and disk formation mechanisms underpins the long-term optical and X-ray variability characteristic of these systems.

Observational evidence supports the truncation of the Be star's disk by the neutron star's tidal forces, which influences disk size, density, and consequent X-ray outburst behavior. The neutron star's strong magnetic field governs the accretion flow geometry and pulsation characteristics, with transitions between sub-critical and super-critical accretion regimes evident in spectral and timing properties.

The ongoing study of Be/X-ray binaries continues to reveal new complexities, including persistent low-luminosity systems and variations in accretion regimes, underscoring the need for coordinated multiwavelength observations. These systems not only enrich our understanding of binary star evolution and high-energy astrophysics but also provide unique testbeds for theoretical models of disk dynamics, mass transfer, and magnetically channeled accretion.

In summary, Be/X-ray binaries are multifaceted astrophysical systems whose detailed study sheds light on fundamental processes in stellar and compact object astrophysics, and sustained observational efforts promise further advances in unraveling their intriguing behaviors.

Funding: This research received no external funding.

Data Availability Statement: Most of the data presented in this study have been published and can be found on the corresponding publication. They are also available on request from the corresponding author.

Acknowledgments: This research has made use of the SIMBAD database, operated at CDS, Strasbourg, France. The optical data were obtained using the facilities at the Skinakas Observatory, which is a joint research facility of the University of Crete and the Foundation for Research and Technology Ž013 Hellas (FORTH).

Conflicts of Interest: The author declares no conflicts of interest.

References

1. Reig, P. Taxonomy of High Mass X-ray binaries from a historical perspective 87th Fujihara Seminar: The 50th Anniversary Workshop of the Disk Instability Model in Compact Binary Stars. 2026. Available online: https://pos.sissa.it/493/023/ (accessed on 24 April 2026).
2. Giacconi, R.; Gursky, H.; Paolini, F.R.; Rossi, B.B. Evidence for x Rays From Sources Outside the Solar System. *Phys. Rev. Lett.* **1962**, *9*, 439.
3. Chodil, G.; Mark, H.; Rodrigues, R.; Seward, F.D.; Swift, C.D. Spectral and Location Measurements of Several Cosmic X-Ray Sources Including a Variable Source in Centaurus. *Phys. Rev. Lett* **1967**, *19*, 681.
4. Giacconi, R.; Gursky, H.; Kellogg, E.; Schreier, E.; Tananbaum, H. Discovery of Periodic X-Ray Pulsations in Centaurus X-3 from UHURU. *Astrophys. J.* **1971**, *167*, L67.
5. Bailer-Jones, C.A.L.; Rybizki, J.; Fouesneau, M.; Demleitner, M.; Andrae, R. Estimating Distances from Parallaxes. V. Geometric and Photogeometric Distances to 1.47 Billion Stars in Gaia Early Data Release 3. *PTA Proc.* **2021**, *161*, 147.
6. Neumann, M.; Avakyan, A.; Doroshenko, V.; Santangelo, A. XRBcats: Galactic High Mass X-ray Binary Catalogue. *Astron. Astrophys.* **2023**, *677*, A134.
7. Fortin, F.; García, F.; Simaz Bunzel, A.; Chaty, S. A catalogue of high-mass X-ray binaries in the Galaxy: From the INTEGRAL to the Gaia era. *Astron. Astrophys.* **2023**, *671*, A149.
8. Kim, V.; Izmailova, I.; Aimuratov. Yerlan Catalog of the Galactic Population of X-Ray Pulsars in High-mass X-Ray Binary Systems. *Astrophys. J. Suppl. Ser.* **2023**, *268*, 21.
9. Shklovsky, I.S. On the Nature of the Source of X-Ray Emission of Sco XR-1. *Astrophys. J.* **1967**, *148*, L1.
10. Burbidge, G. Binary Stars as X-Ray Sources. *Comments Astrophys. Space Phys.* **1972**, *4*, 105.
11. Gursky, H.; Schreier, E. The Binary X-Ray Stars–The Observational Picture. *Symp.-Int. Astron. Union* **1975**, *67*, 413.
12. Maraschi, L.; Treves, A.; van den Heuvel, E.P.J. B-emission Stars and X-ray sources. *Nature* **1976**, *259*, 292.
13. Rappaport, S.; Joss, P.C. Binary X-ray pulsars. *Nature* **1977**, *266*, 123.
14. Truemper, J.; Pietsch, W.; Reppin, C.; Voges, W.; Staubert, R.; Kendziorra, E. Evidence for strong cyclotron line emission in the hard X-ray spectrum of Hercules X-1. *Astrophys. J.* **1978**, *219*, L105.
15. Rappaport, S.; Joss, P.C.; Webbink, R.F. The evolution of highly compact binary stellar systems. *Astrophys. J.* **1982**, *254*, 616.
16. White, N.E. X-ray binaries. *Astron Astrophys. Rev.* **1989**, *1* 85.
17. Stella, L.; White, N.E.; Rosner, R. Intermittent stellar wind accretion and the long-term activity of Population I binary systems containing an X-ray pulsar. *Astrophys. J.* **1986**, *308*, 669.
18. Corbet, R.H.D. The three types of high-mass X-ray pulsator. *Mon. Not. R. Astron. Soc.* **1986**, *220*, 1047.
19. Reig, P.; Roche, P. Discovery of two new persistent Be/X-ray pulsar systems. *Mon. Not. R. Astron. Soc.* **1999**, *306*, 100.
20. Negueruela, I.; Smith, D.M.; Reig, P.; Chaty, S.; Torrejón, J.M. Supergiant Fast X-ray Transients: A New Class of High Mass X-ray Binaries. Unveiled by INTEGRAL. *ESASP* **2006**, *604*, 165.
21. Lopes de Oliveira, R.; Motch, C.; Haberl, F.; Negueruela, I.; Janot-Pacheco, E. New γ Cassiopeiae-like objects: X-ray and optical observations of SAO 49725 and HD 161103. *Astron. Astrophys.* **2006**, *454*, 265.
22. Fortin, F.; García, F.; Simaz Bunzel, A.; Chaty, S. Gamma-ray binaries and related systems. *Astron. Astrophys.* **2013**, *21*, 64.
23. Casares, J.; Negueruela, I.; Ribó, M.; Ribas, I.; Paredes, J.M.; Herrero, A.; Simón-Díaz, S. A Be-type star with a black-hole companion. *Nature* **2014**, *505*, 378.
24. Janssens, S.; Shenar, T.; Degenaar, N.; Bodensteiner, J.; Sana, H.; Audenaert, J.; Frost, A.J. MWC 656 is unlikely to contain a black hole. *Astron. Astrophys.* **2023**, *677*, L9.
25. Revnivtsev, M.; Churazov, E.; Postnov, K.; Tsygankov, S. Quenching of the strong aperiodic accretion disk variability at the magnetospheric boundary. *Astron. Astrophys.* **2009**, *507*, 1211.
26. Mushtukov, A.A.; Lipunova, G.V.; Ingram, A.; Tsygankov, S.S.; Mönkkönen, J.; van der Klis, M. Broad-band aperiodic variability in X-ray pulsars: Accretion rate fluctuations propagating under the influence of viscous diffusion. *Mon. Not. R. Astron. Soc.* **2019**, *486*, 4061.

27. Yang, W.; Wang, W. Millihertz Quasi-Periodic Oscillations in Accreting X-Ray Pulsars. *Universe* **2026**, *12*, 7.
28. Quirrenbach, A.; Bjorkman, K.S.; Bjorkman, J.E.; Hummel, C.A.; Buscher, D.F.; Armstrong, J.T.; Mozurkewich, D.; Elias, N.M., II; Babler, B.L. Constraints on the Geometry of Circumstellar Envelopes: Optical Interferometric and Spectropolarimetric Observations of Seven Be Stars. *Astrophys. J.* **1997**, *479*, 477.
29. Hummel, W.; Vrancken, M. Line formation in Be star circumstellar disks Shear broadening, shell absorption, stellar obscuration and rotational parameter. *Astron. Astrophys.* **2000**, *359*, 1075–1084.
30. Tycner, C.; Lester, J.B.; Hajian, A.R.; Armstrong, J.T.; Benson, J.A.; Gilbreath, G.C.; Hutter, D.J.; Pauls, T.A.; White, N.M. Properties of the Hα-emitting Circumstellar Regions of Be Stars. *Astrophys. J.* **2005**, *624*, 359–371.
31. Grundstrom, E.D.; Gies, D.R. Estimating Be Star Disk Radii using Hα Emission Equivalent Widths. *Astrophys. J.* **2006**, *651*, L53–L56.
32. Porter, J.M.; Rivinius, T. Classical Be Stars. *Publ. Astron. Soc. Pac.* **2003**, *115*, 1153–1170.
33. Rivinius, T. Be Stars: Rapidly Rotating Pulsators. In *Stellar Pulsations. Astrophysics and Space Science Proceedings*; Springer: Berlin/Heidelberg, Germany, 2013; Volume31, p. 253.
34. Frémat, Y.; Zorec, J.; Hubert, A.-M.; Floquet, M. Effects of gravitational darkening on the determination of fundamental parameters in fast-rotating B-type. *Astron. Astrophys.* **2005**, *440*, 305–320.
35. Townsend, R.H.D.; Owocki, S.P.; Howarth, I.D. Be-star rotation: How close to critical? *Mon. Not. R. Astron. Soc.* **2004**, *350*, 189–195.
36. Carciofi, A.C.; Bolzan, G.P.P.; Querido, P.R.; Rubio, A.C.; Labadie-Bartz, J.; de Amorim, T.H.; Fonseca Silva, A.C.; Schiavolim, V.L. Mass Loss in Be Stars: News from Two Fronts. *Galaxies* **2025**, *13*, 77.
37. Baade, D.; Rivinius, T.; Pigulski, A.; Carciofi, A.; Handler, G.; Kuschnig, R.; Martayan, C.; Mehner, A.; Moffat, A.F.J.; Pablo, H.; et al. Pulsations and outbursts in Be stars: Small differences–big impacts. *PTA Proc.* **2017**, *5*, 196–205.
38. Baade, D.; Rivinius, T.; Pigulski, A.; Panoglou; Despina; Carciofi, A.; Handler, G.; Kuschnig, R.; Martayan, C.; Mehner, A.; et al. BRITEning up the Be Phenomenon. *PTA Proc.* **2018**, *8*, 69–76.
39. Baade, D.; Rivinius, T.; Pigulski, A.; Carciofi, A.C.; Martayan, C.; Moffat, A.F.J.; Wade, G.A.; Weiss, W.W.; Grunhut, J.; Handler, G.; et al. Short-term variability and mass loss in Be stars. I. BRITE satellite photometry of η and μ Centauri. *Astron. Astrophys.* **2016**, *588*, A56.
40. Semaan, T.; Hubert, A.M.; Zorec, J.; Gutiérrez-Soto, J.; Frémat, Y.; Martayan, C.; Fabregat, J.; Eggenberger, P. Study of a sample of faint Be stars in the exofield of CoRoT. II. Pulsation and outburst events: Time series analysis of photometric variations. *Astron. Astrophys.* **2018**, *613*, A70.
41. Balona, L.A.; Ozuyar, D. TESS Observations of Be Stars: General Characteristics and the Impulsive Magnetic Rotator Model. *Astrophys. J.* **2021**, *921*, 5.
42. Baade, D. There are more absorption line profile-variable Be stars with short periods. *Astron. Astrophys.* **1984**, *134*, 105.
43. Rivinius, T.; Baade, D.; Štefl, S. Non-radially pulsating Be stars. *Astron. Astrophys.* **2003**, *411*, 229–247.
44. Zima, W. A new method for the spectroscopic identification of stellar non-radial pulsation modes. I. The method and numerical tests. *Astron. Astrophys.* **2006**, *455*, 227.
45. Reig, P.; Fabregat, J. Fast time optical variability in Be/X-ray binaries. Pulsation and rotation *Astron. Astrophys.* **2022**, *667*, A18.
46. Labadie-Bartz, J.; Carciofi, A.C.; Henrique de Amorim, T.; Rubio, A.; Luiz Figueiredo, A.; Ticiani dos Santos, P.; Thomson-Paressant, K. Classifying Be Star Variability With TESS. I. The Southern Ecliptic. *Astron. J.* **2022**, *163*, 226.
47. Panoglou, D.; Carciofi, A.C.; Vieira, R.G.; Cyr, I.H.; Jones, C.E.; Okazaki, A.T.; Rivinius, T. Be discs in binary systems–I. Coplanar orbits. *Mon. Not. R. Astron. Soc.* **2016**, *461*, 2616–2629.
48. Cyr, I.H.; Jones, C.E.; Panoglou, D.; Carciofi, A.C.; Okazaki, A.T. Be discs in binary systems–II. Misaligned orbits. *Mon. Not. R. Astron. Soc.* **2017**, *471*, 596–605.
49. Rubio, A.C.; Carciofi, A.C.; Bjorkman, J.E.; de Amorim, T.H.; Okazaki, A.T.; Suffak, M.W.; Jones, C.E.; Candido, P.P. High-spatial-resolution simulations of Be star disks in binary systems: I. Structure and kinematics of coplanar disks. *Astron. Astrophys.* **2025**, *698*, A309.
50. Reig, P.; Fabregat, J. Long-term variability of high-mass X-ray binaries. I. Photometry. *Astron. Astrophys.* **2015**, *574*, A33.
51. Reig, P.; Nersesian, A.; Zezas, A.; Gkouvelis, L.; Coe, M.J. Long-term optical variability of high-mass X-ray binaries. II. Spectroscopy. *Astron. Astrophys.* **2016**, *590*, A122.
52. Reig, P.; Blinov, D.; Tzouvanou, A. Long-term optical variability of high-mass X-ray binaries. III. Polarimetry. *Astron. Astrophys.* **2026**, *708*, A266.
53. Reig, P.; Fabregat, J.; Coe, M.J. A new correlation for Be/X-ray binaries: the orbital period-Hα equivalent width diagram. *Astron. Astrophys.* **1997**, *322*, 193–196.
54. Okazaki, A.T.; Negueruela, I. A natural explanation for periodic X-ray outbursts in Be/X-ray binaries. *Astron. Astrophys.* **2001**, *377*, 161.

55. Okazaki, A.T.; Bate, M.R.; Ogilvie, G.I.; Pringle, J. E Viscous effects on the interaction between the coplanar decretion disc and the neutron star in Be/X-ray binaries. *Mon. Not. R. Astron. Soc.* **2002**, *337*, 967.
56. Brown, R.O.; Coe, M.J.; Ho, W.C.G.; Okazaki, A.T. Modelling decretion discs in Be/X-ray binaries. *Mon. Not. R. Astron. Soc.* **2019**, *488*, 387.
57. Martin, R.G.; Lubow, S.H.; Armitage, P.J.; Price, D.J. Decretion disc size in Be/X-ray binaries depends upon the disc aspect ratio. *Mon. Not. R. Astron. Soc.* **2024**, *530*, 4148–4152.
58. Halonen, R.J.; Jones, C.E. On the Intrinsic Continuum Linear Polarization of Classical Be Stars during Disk Growth and Dissipation. *Astrophys. J.* **2013**, *765*, 17.
59. Yudin, R.V. Statistical analysis of intrinsic polarization, IR excess and projected rotational velocity distributions of classical Be stars. *Astron. Astrophys.* **2001**, *368*, 912–931.
60. Weng, S.-S.; Ji, L. X-Ray Views of Galactic Accreting Pulsars in High-Mass X-Ray Binaries. *Univers* **2024**, *10*, 453.
61. Harmanec, P. Review of observational facts about Be stars. *Hvar. Obs. Bull.* **1983**, *7*, 55.
62. Hanuschik, R.W. Shell lines in disks around Be stars. 1: Simple approximations for Keplerian disks. *Astron. Astrophys.* **1995**, *295*, 423–434.
63. Chhotaray, B.; Naik, S.; Jaisawal, G.K.; Ahuja, G. Optical and X-ray studies of the Be/X-ray binary IGR J06074+2205. *Mon. Not. R. Astron. Soc.* **2024**, *534*, 2830–2847.
64. Staubert, R.; Trümper, J.; Kendziorra, E.; Klochkov, D.; Postnov, K.; Kretschmar, P.; Pottschmidt, K.; Haberl, F.; Rothschild, R.E.; Santangelo, A.; et al. Cyclotron lines in highly magnetized neutron stars. *Astron. Astrophys.* **2019**, *622*, A61.
65. Raichur, H.; Paul, B. Apsidal motion in 4U0115+63 and orbital parameters of 2S1417-624 and V0332+53. *Mon. Not. R. Astron. Soc.* **2010**, *406*, 2663–2670.
66. Malacaria, C.; Jenke, P.; Roberts, O.J.; Wilson-Hodge, C.A.; Cleveland, W.H.; Mailyan, B. GBM Accreting Pulsars Program Team The Ups and Downs of Accreting X-Ray Pulsars: Decade-long Observations with the Fermi Gamma-Ray Burst Monitor. *Astrophys. J.* **2020**, *896*, 90.
67. Alpar, M.A.; Shaham, J. Is GX5–1 a millisecond pulsar? *Nature* **1985**, *316*, 239–241.
68. van der Klis, M.; Stella, L.; White, N.; Jansen, F.; Parmar, A.N. Intensity and Source State Dependence of the Quasi-periodic Oscillations in Scorpius X-1. *Astrophys. J.* **1987**, *316*, 411.
69. Ma, R.; Tao, L.; Zhang, S.-N.; et al. High energy millihertz quasi-periodic oscillations in 1A 0535 + 262 with Insight-HXMT challenge current models. *Mon. Not. R. Astron. Soc.* **2022**, *517*, 1988–1999.
70. Shirakawa, A.; Lai, D.M. Magnetically Driven Precession of Warped Disks and Millihertz Variabilities in Accreting X-Ray Pulsars *Astrophys. J.* **2002**, *565*, 1134–1140.
71. Reig, P. Rapid spectral and timing variability of Be/X-ray binaries during type II outbursts. *Astron. Astrophys.* **2008**, *489*, 725–740.
72. Reig, P.; Nespoli, E. Patterns of variability in Be/X-ray pulsars during giant outbursts. *Astron. Astrophys.* **2013**, *551*, A1.
73. Doroshenko, V.; Zhang, S.N.; Santangelo, A.; Ji, L.; Tsygankov, S.; et al. Hot disc of the Swift J0243.6+6124 revealed by Insight-HXMT. *Mon. Not. R. Astron. Soc.* **2020**, *491*, 1857–1867.
74. Reig, P.; Ma, R.C.; Tao, L.; Zhang, S.; Zhang, S.N.; Doroshenko, V. X-ray spectral-timing variability of 1A 0535+262 during the 2020 giant outburst. *Astron. Astrophys.* **2022**, *659*, A178.
75. Li, P.P.; Tao, L.; Ma, R.C.; Ge, M.Y.; Zhao, Q.C.; et al. Broad-band noise and quasi-periodic oscillation characteristics of the X-ray pulsar RX J0440.9+4431. *Mon. Not. R. Astron. Soc.* **2024**, *529*, 1187–1194.
76. Motch, C.; Stella, L.; Janot-Pacheco, E.; Mouchet, M. Accretion Mechanisms in the Be/X-Ray Transient System A0535+26. *Astrophys. J.* **1991**, *369*, 490.
77. Okazaki, A.T.; Hayasaki, K.; Moritani, Y. Origin of Two Types of X-Ray Outbursts in Be/X-Ray Binaries. I. Accretion Scenarios. *Publ. Astron. Soc. Jpn.* **2013**, *65*, 41.
78. Martin, R.G.; Nixon, C.; Armitage, P.J.; Lubow, S.H.; Price, D.J. Giant Outbursts in Be/X-Ray Binaries. *Astrophys. J.* **2014**, *790*, L34.
79. Monageng, I.M.; McBride, V.A.; Coe, M.J.; Steele, I.A.; Reig, P. On the relationship between circumstellar disc size and X-ray outbursts in Be/X-ray binaries. *Mon. Not. R. Astron. Soc.* **2017**, *464*, 572–585.
80. Kozai, Y. Secular perturbations of asteroids with high inclination and eccentricity. *Astron. J.* **1962**, *67*, 591–598.
81. Lidov, M.L. The evolution of orbits of artificial satellites of planets under the action of gravitational perturbations of external bodies. *Planet. Space Sci.* **1962**, *9*, 719–759.
82. Martin, R.G.; Nixon, C.; Lubow, S.H.; Armitage, P.J.; Price, D.J.; Doğan, S.; King, A. The Kozai-Lidov Mechanism in Hydrodynamical Disks. *Astrophys. J.* **2014**, *792*, L33.
83. Fu, W.; Lubow, S.H.; Martin, R.G. The Kozai-Lidov Mechanism in Hydrodynamical Disks. II. Effects of Binary and Disk Parameters. *Astrophys. J.* **2015**, *807*, 75.
84. Negueruela, I.; Reig, P.; Finger, M.H.; Roche, P. Detection of X-ray pulsations from the Be/X-ray transient A 0535+26 during a disc loss phase of the primar. *Astron. Astrophys.* **2000**, *356*, 1003–1009.

85. Reig, P.; Zezas, A. Disc-loss episode in the Be shell optical counterpart to the high-mass X-ray binary IGR J21343+4738. *Astron. Astrophys.* **2014**, *561*, A137.
86. Reig, P.; Doroshenko, V.; Zezas, A. The quiescent state of the accreting X-ray pulsar SAX J2103.5+4545. *Mon. Not. R. Astron. Soc.* **2014**, *445*, 1314–1320.
87. Tsygankov, S.S.; Wijnands, R.; Lutovinov, A.A.; Degenaar, N.; Poutanen, J. The X-ray properties of Be/X-ray pulsars in quiescence. *Mon. Not. R. Astron. Soc.* **2017**, *470*, 126–141.
88. Davidson, K.; Ostriker, J.P. Neutron-Star Accretion in a Stellar Wind: Model for a Pulsed X-Ray Source. *Astrophys. J.* **1973**, *179*, 585–598.
89. Basko, M.M.; Sunyaev, R.A. The limiting luminosity of accreting neutron stars with magnetic fields. *Mon. Not. R. Astron. Soc.* **1976**, *175*, 395–417.
90. Lyubarskii, Y.E.; Syunyaev, R.A. Comptonization in a Radiation Dominated Shock and the Spectra of X-Ray Pulsars. *Sov. Astron. Lett.* **1982**, *8*, 330–335.
91. Burnard, D.J.; Arons, J.; Klein, R.I. Accretion Powered Pulsars: Continuum Spectra and Light Curves of Settling Accretion Mounds. *Astrophys. J.* **1991**, *367*, 575.
92. Harding, A.K. Emission Processes in X-ray Pulsars. *AIP Conf. Proc.* **1994**, *308*, 429.
93. Wilson-Hodge, C.A.; Malacaria, C.; Jenke, P.A.; Jaisawal, G.K.; Kerr, M.; et al. NICER and Fermi GBM Observations of the First Galactic Ultraluminous X-Ray Pulsar Swift J0243.6+6124. *Astrophys. J.* **2018**, *863*, 9.
94. Ji, L.; Ducci, L.; Santangelo, A.; Zhang, S.; Suleimanov, V.; et al. Switches between accretion structures during flares in 4U 1901+03. *Mon. Not. R. Astron. Soc.* **2020**, *493*, 5680–5692.
95. Becker, P.A.; Klochkov, D.; Schönherr, G.; Nishimura, O.; Ferrigno; et al. Spectral formation in accreting X-ray pulsars: Bimodal variation of the cyclotron energy with luminosity. *Astron. Astrophys.* **2012**, *544*, A123.
96. Mushtukov, A.A.; Tsygankov, S.S.; Serber, A.V.; Suleimanov, V.F.; Poutanen, J. Positive correlation between the cyclotron line energy and luminosity in sub-critical X-ray pulsars: Doppler effect in the accretion channel. *Mon. Not. R. Astron. Soc.* **2015**, *454*, 2714–2721.
97. Serim, M.M.; Özüdoğru, Ö.C.; Dönmez, Ç.K.; Şahiner, Ş.; Serim, D.; Baykal, A.; İnam, S.Ç. Timing and spectral analysis of 2S 1417-624 during its 2018 outburst. *Mon. Not. R. Astron. Soc.* **2022**, *510*, 1438–1449.
98. Mandal, M.; Sharma, R.; Pal, S.; et al. Probing spectral and timing properties of the X-ray pulsar RX J0440.9 + 4431 in the giant outburst of 2022-2023. *Mon. Not. R. Astron. Soc.* **2023**, *526*, 771–781.

Disclaimer/Publisher's Note: The statements, opinions and data contained in all publications are solely those of the individual author(s) and contributor(s) and not of MDPI and/or the editor(s). MDPI and/or the editor(s) disclaim responsibility for any injury to people or property resulting from any ideas, methods, instructions or products referred to in the content.